Available online at www.sciencedirect.com
ScienceDirect
Physics Procedia 3 (2010) 1249–1254
Physics Procedia
www.elsevier.com/locate/procedia

Weak localization properties of graphene with intrinsic and Rashba spin-orbit couplings

Ken-Ichiro Imura, Yoshio Kuramoto, Kentaro Nomura

Department of Physics, Tohoku University, Sendai 980-8578, Japan

Abstract

We propose the notion of counting the number of *activated* spins to identify the weak localization properties of graphene under effects of inter-valley scattering, intrinsic and Rashba spin-orbit interactions (SOI). It is predicted that perpendicular electric field due to gate voltage of the substrate drives the system to anti-localization by enhancing the Rashba SOI.

Keywords: graphene, weak localization, spin-orbit coupling, topological insulator

1. Introduction

Graphene has a strong tendency *not to localize* [1, 2], reflecting its Dirac nature [3]. Together with the absence of backward scattering, AL in graphene is a clear manifestation of Berry phase π. Inter-valley scattering, on the other hand, drives the system from AL to WL [1]. Experiments show also a unitary behavior [4]. Here, we report our recent study on the localization properties of graphene in the presence of intrinsic and Rashba spin-orbit interactions (SOI) [5].

As a concrete model, we employ doped and disordered Kane-Mele model, the latter proposed as the first implementation of Z_2 topological insulator [7]. The Kane-Mele model has a three story structure, depicted in Table 1. In the continuum limit, it is described by the Hamiltonian: $H_{KM} = H_1 + H_\Delta + H_R$, consisting of the following three elements: (i) graphene in the massless limit: $H_1 = \hbar v_F(p_x\sigma_x\tau_z + p_y\sigma_y)$, (ii) topological mass term, encoding the intrinsic spin-orbit interaction: $H_\Delta = -\Delta\sigma_z\tau_z s_z$, (iii) Rashba term, playing the role of activating the real spin degree of freedom: $H_R = -\lambda_R(\sigma_x\tau_z s_y - \sigma_y s_x)/2$, each describing the corresponding floor of the three story structure. Note that the Kane-Mele model has also the valley degree of freedom, corresponding to two Dirac points of graphene: K and K'. The ionic mass term is induced by parity (AB sublattice symmetry) breaking staggered chemical potential. For comparison with H_Δ, we consider also ionic mass term $H_m = m\sigma_z$. The Kane-Mele model thus possesses three types of pseudo or real spins, represented by Pauli's matrices, $\vec{\sigma}$, $\vec{\tau}$ and $\vec{s}$, operating in different subspaces: $\vec{\sigma}$ acts on the sublattice spin A-B, $\vec{\tau}$ on the valley spin K-K', and $\vec{s}$ on the real spin.

doi:10.1016/j.phpro.2010.01.171

Table 1: Three story structure of Kane-Mele Z_2 topological insulator, and its WL properties under doping. LRS is equivalent to the single valley model. The parity of N_s, the number of activated spin degrees of freedom, determines its WL properties: standard WL (orthogonal) or AL (symplectic). Broken TRS leads to U (unitary) behavior.

	LRS (single valley)	SRS (K-K' coupled)
(i) massless graphene: $H_1 = p_x\sigma_x\tau_z + p_y\sigma_y$	$N_s = 1$ (AB) $\to$ AL	$N_s = 2$ (AB,KK') $\to$ WL
(ii) mass terms: $H_2 = H_1 + H_{\Delta,m}$	unitary	(a) unitary
(a) topological $-\Delta\sigma_z\tau_z s_z$ vs. (b) ionic $m\sigma_z$	no $1/g$-correction	(b) $N_s = 2$ (AB,KK') $\to$ WL
(iii) Rashba spin-orbit interaction:	(a) $N_s = 2$ (AB, real spin) $\to$ WL	$N_s = 3$ (AB, KK', real spin) $\to$ AL
$H_3 = H_2 - \lambda_R(\sigma_x\tau_z s_y - \sigma_y s_x)/2$	(b) unitary	

Table 2: Time reversal operations T_Σ, relevant in the subspace spanned by activated spins. Transformation property of a mass term $O = m\sigma_z$, $\Delta\sigma_z\tau_z s_z$ under T_Σ: $T_\Sigma O T_\Sigma^{-1} = \pm O$. The sign appears in the table. U refers to unitary class.

activated spins	$\vec{\sigma}$	$\vec{\sigma}, \vec{\tau}$	$\vec{\sigma}, \vec{s}$	$\vec{\sigma}, \vec{\tau}, \vec{s}$
relevant TRS operation	T_σ	$T_{\sigma\tau}$	$T_{\sigma s}$	$T_{\sigma\tau s}$
σ_z	$- \to U$	$+$	$- \to U$	$+$
$\Delta\sigma_z\tau_z s_z$	$- \to U$	$- \to U$	$+$	$+$

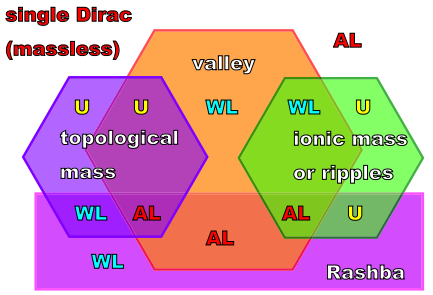

Figure 1: Weak localization classes of graphene and Z_2 topological insulator with different types of the mass and impurity scattering. WL, AL and U refer to weak localization (orthogonal class), weak anti-localization (symplectic class) and absence of WL (unitary class), respectively.

2. Symmetry considerations

The results of our analyses are also summarized in Table 1, but more schematically represented in Figure 1. The latter shows localization classes: WL, AL, and U depending on the inter-valley scattering, types of the mass term, and the Rashba SOI. Without these effects, the system becomes massless and belongs to AL [1, 2]. Note that, in the presence of inter-valley scattering, crossovers to AL occurs by switching on the Rashba SOI. This crossover is achieved by controlling the gate voltage of the substrate on which the system is placed. Inter-valley coupling, on the other hand, is determined by the range of impurity potential [8]. Long-range scatterers (LRS) do not involve intervalley scattering, whereas short-range scatterers (SRS) activates the valley spin.

Figure 1 is also relevant to *intrinsic* single valley systems [9], such as the one realized in HgTe/CdTe quantum well [10]. In the latter system, a single pair (Kramers pair) of Dirac cones appear, in contrast to graphene. Note that two Dirac cones (a Kramers pair, with real spin $\uparrow$ and $\downarrow$), described in the model introduced in Ref. [9], have the *same* sign for their mass term, implying (superficially) the ordinary (ionic) mass case in our language. However, they have also different chiralities, and by a simple linear transformation (exchange of rows and columns), they can be mapped, and indeed corresponds to the topological mass case, studied in Sec. IV A. Our diagnosis (see Table 1, and also FIG. 1) suggests that the single-valley HgTe/CdTe system shows a crossover from unitary to orthogonal (WL) symmetry class, on activating the real spin degrees of freedom by a (Rashba-like) off-diagonal interaction between real spin $\uparrow$ and $\downarrow$ sectors.

As shown in Table 1, sublattice spin $\vec{\sigma}$ is always active, whereas valley and real spins can be switched on and off, leading to four different cases for the subspace Σ spanned by active spins. In order to distinguish active and inactive spins, we introduce (pseudo) TRS operations T_Σ, defined in the subspace Σ of activated spins, where $\Sigma = \{\vec{\sigma}\}, \{\vec{\sigma}, \vec{\tau}\}, \{\vec{\sigma}, \vec{s}\}, \{\vec{\sigma}, \vec{\tau}, \vec{s}\}$. Note that in the subspace Σ, the total Hamiltonian including the scattering potential becomes block diagonal, since it has no off-diagonal components in the space of inactivated spins. The relevant TRS operation T_Σ *leaves each of such blocks invariant*. The relevant TRS operations are given explicitly as,

$$\begin{aligned} T_\sigma &= -i\sigma_y C, \quad T_{\sigma\tau} = \tau_x C, \\ T_{\sigma s} &= (-i\sigma_y)(-is_y)C, \quad T_{\sigma\tau s} = \tau_x(-is_y)C, \end{aligned} \tag{1}$$

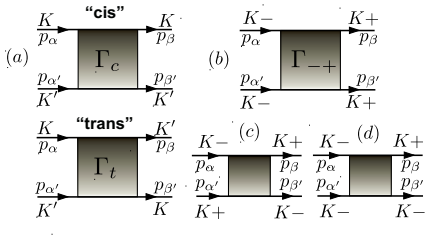

Figure 2: Particle-particle ladders. (a) Relevant diagrams in the presence of short-range scatterers (SRS). "cis" and "trans" refers to specific configurations of the valleys. (b-d) Bare diagrams involving *inter-branch* processes ($\lambda_R \neq 0$, no SRS). (b) γ_{-+} contributes to $1/q^2$-singularity, whereas such diagrams as (c) and (d) are irrelevant to the singularity, since $p_\alpha + p_{\alpha'}$ cannot be smaller than the order of λ_R.

where C is complex conjugation. $T_{\sigma\tau s}$ represents the genuine TRS operation. Effective TRS of the system is, therefore, determined by the transformation property of the mass term (see TABLE II). When a mass term is odd against TRS, the system shows the unitary behavior. Four unitary phases in FIG.1 correspond to the four minus signs in TABLE II. If some (pseudo or genuine) TRS exists in the system, its weak localization property is determined by the number N_s of the activated spin degrees of freedom. One can verify $T_\Sigma^2 = 1$ if N_s is even, whereas $T_\Sigma^2 = -1$ if N_s is odd. The former (latter) corresponds to the orthogonal (symplectic) class in the random matrix theory, and leads to constructive (destructive) interference between two scattering processes transformed from one to the other by T_Σ.

In the presence of a mass term, irrespective of its type, one finds unitary behavior for LRS. Scattering matrix elements are *diagonal* in $\vec{\tau}$-space, and $\vec{\sigma}$ is the only active spin ($N_s = 1$, TRS broken). In the massless case, a pseudo TRS operation T_σ mimics the role of genuine TRS. Once TRS is effectively restored, the system's WL property is determined by the parity of N_s. The mass term, on the other hand, explicitly breaks T_σ.

The SRS activate the valley spin $\vec{\tau}$ ($N_s = 2$), since its matrix elements involve off-diagonal terms in this subspace. In the case of ionic mass term, this leads the system to standard WL, since activation of the valley spin $\vec{\tau}$ restores the (pseudo) TRS. In the case of topological mass term, the system stays unitary, since restoration of TRS needs also the activation of real spin $\vec{s}$. The latter is embodied by the Rashba SOI. In the presence of both SRS and Rashba SOI, we predict AL, since $N_s = 3$.

3. Weak localization corrections

Let us go into some details of diagrammatic calculations. We first consdier the case of $\lambda_R = 0$. In the presence of topological mass term H_Δ, The spinor part of the conduction band eigenstates reads,

$$|K\alpha\rangle = \begin{bmatrix} \cos\frac{\theta_\alpha}{2} \\ e^{i\phi_\alpha}\sin\frac{\theta_\alpha}{2} \end{bmatrix}, |K'\alpha\rangle = \begin{bmatrix} e^{i\phi_\alpha}\sin\frac{\theta_\alpha}{2} \\ -\cos\frac{\theta_\alpha}{2} \end{bmatrix}, \tag{2}$$

where α specifies a three-dimensional fictitious momentum $\vec{p} = (p_x, p_y, -\Delta)$, and the polar angles θ, ϕ satisfy $\cos\theta = -\Delta/\sqrt{p_x^2 + p_y^2 + \Delta^2}$, $\cos\phi = p_x/\sqrt{p_x^2 + p_y^2}$.

The LRS have a potential range much larger than the inter-atomic distance, and do not couple K and K'. The system cannot see the difference between two types of mass term, both showing unitary behavior, i.e., the diffusion type singularity is cut off by a cooperon's lifetime. This unitary phase shows a crossover to the well-established symplectic behavior of graphene in the single Dirac cone [1, 2].

The SRS involve inter-valley scattering, allowing for distinguishing the two different types of mass term: topological and ionic. The scattering matrix elements involve a projection operator in the AB sublattice space, $\mathcal{P}_{A,B}$. As for the singular contribution, one can focus on the two types of diagrams shown in FIG.1. The "trans" component γ_t reads explicitly,

$$\begin{aligned}\gamma_t &= 2\pi\nu n_A u_A^2 \langle K'\beta|\mathcal{P}_A\tau_-|K\alpha\rangle\langle K\beta'|\mathcal{P}_A\tau_+|K'\alpha'\rangle \\ &+ 2\pi\nu n_B u_B^2 \langle K'\beta|\mathcal{P}_B\tau_-|K\alpha\rangle\langle K\beta'|\mathcal{P}_B\tau_+|K'\alpha'\rangle \\ &= -e^{i(\phi_\alpha-\phi_\beta)}\eta_S \sin^2\theta/2 \ (=-\gamma_c), \end{aligned} \tag{3}$$

where we have introduced $\eta_S = 2\pi\nu(n_A u_A^2 + n_B u_B^2)/2$, with ν, $n_{A,B}$ and $u_{A,B}$ being, respectively, the density of states, the impurity density and the typical strength of scattering potential at the A (B) sites. γ_t has an additional minus sign, which plays the role of driving the crossover from symplectic to orthogonal behavior in the massless limit [1]. The Bethe-Salpeter equation (BSE) takes the form of two coupled equations:

$$\begin{bmatrix} \Gamma_c \\ \Gamma_t \end{bmatrix}_{\alpha\beta} = \begin{bmatrix} \gamma_c \\ \gamma_t \end{bmatrix}_{\alpha\beta} + \begin{bmatrix} \gamma_c & \gamma_t \\ \gamma_t & \gamma_c \end{bmatrix}_{\alpha\mu} \Pi_\mu \begin{bmatrix} \Gamma_c \\ \Gamma_t \end{bmatrix}_{\mu\beta} \tag{4}$$

After diagonalization, one finds, $\Gamma_c + \Gamma_t = 0$, and $\left[1 - (\gamma_c^{(1)} - \gamma_t^{(1)})\Pi_S\right](\Gamma_c - \Gamma_t) = \gamma_c - \gamma_t$, where $\Pi_S \simeq \tau_S(1 - \tau_S D q^2)$ with $\tau_S = 1/\eta_S$ being the scattering time. We also introduced $\gamma_{c,t}^{(1)}$ in the light of a general expression: $\gamma = \sum_l \gamma^{(l)} e^{il(\phi_\alpha-\phi_\beta)}$. Cancellation between τ_S and the bare γ's is incomplete, giving a finite lifetime. The system shows a unitary behavior, irrespective of the preserved TRS of underlying Hamiltonian $H = H_1 + H_\Delta$. $1/q^2$-singularity is recovered in the limit $E \to \infty$ (orthogonal class).

Rashba SOI appears when inversion symmetry with respect to the 2D plane is broken, say, by a perpendicular electric field. Rashba SOI lifts the two-fold real spin degeneracy of the two conduction and two valence bands. The conduction bands $E_\pm$ have an energy dispersion: $E_\pm = \sqrt{p_x^2 + p_y^2 + (\Delta \pm \lambda_R/2)^2} \pm \lambda_R/2$. We introduce fictitious 3D momentum: $\vec{p}_\pm = (p_x, p_y, \Delta \pm \lambda_R/2)$, and parametrize eigen spinors $|K\pm\rangle$ in terms of polar angles satisfying, $\cos\theta_\pm = (\Delta \pm \lambda_R/2)/\sqrt{p_x^2 + p_y^2 + (\Delta \pm \lambda_R/2)^2}$. Rashba coupling imposes a stronger constraint on the choice of our basis. As a result, the matrix element, such as, $\langle K\beta|1|K\alpha\rangle = \cos(\phi_\alpha - \phi_\beta)\sin^2(\theta_-/2) + \cos^2(\theta_-/2)$, becomes *real* (no Berry phase). space0.3 cm

When $E > \Delta + \lambda_R$, inter-branch matrix elements plays a role. They modify the scattering time $\tau_\pm$ for the $|K\pm\rangle$ branches. As for particle-particle ladders, such as FIG.2 (b), four electron states α, β, α', β' can, in principle, take either of the two channel indices, $|K-\rangle$ or $|K+\rangle$, generating eight types of diagrams in total. However, a simplification is possible at this level: since we are interested only in the $1/q^2$-singular part of cooperon diagrams, we need $p_\alpha + p_{\alpha'} = q \simeq 0$. This means that α and α' must belong to the same branch. We can thus safely focus on such diagrams as γ_{+-} and γ_{-+} depicted in FIG.2 (b), or even simpler γ_{--} and γ_{++}. Other γ's such as FIG.2 (c) and (d) are irrelevant to $1/q^2$ singularity. Explicit form of relevant γ's are given as,

$$\gamma_{\pm\pm} = \eta_L\Big[\cos^2(\phi_\alpha - \phi_\beta)\sin^4\frac{\theta_\pm}{2}$$

$$+ \quad 2\cos^2(\phi_\alpha - \phi_\beta)\sin^2\frac{\theta_\pm}{2}\cos^2\frac{\theta_\pm}{2} + \cos^4\frac{\theta_\pm}{2}\Big]$$

$$\gamma_{\pm\mp} = -\eta_L \sin^2(\phi_\alpha - \phi_\beta)\sin\frac{\theta_+}{2}\sin\frac{\theta_-}{2}. \tag{5}$$

These four types of diagrams satisfy coupled BSE. But its 4×4 coupling matrix is shown to be block diagonalizable. One can, e.g., decouple Γ_{--} and Γ_{+-}, from the remaining part. To identify the singular contribution, we employ the expansion into different angular momentum contributions, and pick up only the $l = 0$ component. The dressed cooperons show indeed $1/q^2$-singularity at the $l = 0$ channel. Rashba SOI thus drives the system to standard WL, whenever the Fermi level is above the gap.

What happens if one adiabatically switches *off* the Rashba term? The simplification we have made for justifying the decoupling of Γ_{--} and Γ_{+-} is no longer valid. In the limit of vanishing λ_R we cannot simply neglect such diagrams as FIG.1 (c), (d). They could contribute equally to the $1/q^2$ singularity if the singularity ever appears. Relations such as $p_\alpha + p_{\alpha'} = q \simeq 0$ can be satisfied in these diagrams. In the coupled BSE, the cooperons acquire more channels to couple to, and one can no longer decouple Γ_{--} and Γ_{+-}. As a result, the cancellation property between particle-particle ladders and the self-energy is lost. The loss of cancellation property immediately leads to the absence of WL. On the contrary, if one starts from the situation where Rashba SOI is absent in the first place, it is possible to choose a basis in which that two (degenerate) channels are decoupled.

We finally consider the case of SRS in the presence of Rashba SOI ($\lambda_R \neq 0$). One finds in this case the *cancellation* between the self-energy and γ at the $l = 0$ channel. But here additional minus sign analogous to Eq.(3) appears due to inter-valley scattering, driving the system to AL.

4. Concluding remarks

For the crossover to be experimentally accessible, Rashba SOI needs to be the order of $\sim$ 1 K. This corresponds to the electric field of order $\sim$ 1V/nm, a value attainable in double-gated graphene devices [11]. The crossover to AL will be observed for a sample with insignificant ripples. A similar crossover due to Rashba SOI has been observed in another context in InGaAs/InAlAs quantum well [12].

In conclusion, we propose the notion of counting the number of activated spins to identify systems' weak localization property. Providing such a simple scenario, our diagnosis serves as a contemporary version of the weak localization theory.

[1] H. Suzuura, T. Ando, Phys. Rev. Lett. **89** (2002) 266603.
[2] K. Nomura, M. Koshino, S. Ryu, Phys. Rev. Lett. **99** (2007) 146806.
[3] A. K. Geim, K. S. Novoselov, Nat. Mater. **6** (2007) 183.
[4] S.V. Morozov, et al., Phys. Rev. Lett. **97** (2006) 016801.
[5] K.-I. Imura, Y. Kuramoto and K. Nomura, Phys. Rev. B **80**, 085119 (2009).
[6] S. Hikami, A.I. Larkin, Y. Nagaoka, Prog. Theor. Phys. **63** (1980) 707.
[7] C.L. Kane, E.J. Mele, Phys. Rev. Lett. **95** (2005) 146802; ibid., 226801.
[8] T. Nakanishi, T. Ando, J. Phys. Soc. Jpn. **68** (1999) 561 .
[9] B. A. Bernevig, et al., Science **314** (2006) 1757.
[10] M. König et al., Science **318** (2007) 766.
[11] J.B. Oostinga, et al., Nature Materials **7** (2007) 151.
[12] T. Koga, J. Nitta, T. Akazaki, H. Takayanagi, Phys. Rev. Lett. **89** (2002) 046801.